Applied Catalysis B: Environmental 180 (2016) 199–209

Contents lists available at ScienceDirect

Applied Catalysis B: Environmental

journal homepage: www.elsevier.com/locate/apcatb

The electrochemical reduction of nitrate over micro-architectured metal electrodes with stainless steel scaffold

Jenn Fang Su [a], Inci Ruzybayev [b], Ismat Shah [b,c], C.P. Huang [a,*]

[a] Department of Civil and Environmental Engineering, University of Delaware, Newark, DE 19716, USA
[b] Department of Physics and Astronomy, University of Delaware, Newark, DE 19716, USA
[c] Department of Materials Science and Engineering, University of Delaware, Newark, DE 19716, USA

ARTICLE INFO

Article history:
Received 7 April 2015
Received in revised form 6 June 2015
Accepted 16 June 2015
Available online 20 June 2015

Keywords:
Nitrate reduction
Bimetallic
Cu/SS
Pd–Cu/SS
Nitrogen

ABSTRACT

Cu and Pd–Cu (Pd = 40 wt%) electrodes supported on stainless steel (Cu/SS and Pd–Cu/SS) were prepared using electrodeposition methods and characterized by X-ray diffraction, scanning electron microscope, and X-ray photoelectron spectroscopy. The electrocatalytic reduction of nitrate on Cu/SS and Pd–Cu/SS electrodes was studied in sodium perchlorate electrolyte. By tuning the applied potential, nitrate was found to be selectively reduced to different products, indicating a strong dependence of nitrate reduction reaction on the applied potential. Moreover, the effect of electrode material on nitrate reduction was studied also. Results showed that the nitrate reduction over the two electrodes was different due in part to distinct surface morphology. Results demonstrated a novel avenue to improve the selectivity of nitrate reduction products through controlling the applied potential and selection of electrode material. Results also showed strategy warrant further studies on nitrate conversion to harmless nitrogen gas.

1. Introduction

Nitrate is a known harmful chemical species commonly present in natural water systems such as ground water, lakes, and rivers [1]. High nitrate level in drinking water can cause methemoglobinemia in infants and gastrointestinal cancer in adults [2,3]. The World Health Organization (WHO) has proposed a maximum nitrate concentration of 50 ppm in drinking water [4]. Therefore, the removal of nitrate from water has drawn considerable attention from the water supply industry. In order to develop sustainable water purification technology, it is reasonable to convert nitrate to gaseous N_2 directly without other byproducts especially ammonia, which requires further separation [5]. Biological denitrification is able to selectively transform nitrate into harmless N_2 [6]. However, the success of the process, mostly dependent on bacterial activities, has relatively low reaction rate, produces undesired byproducts, and requires precision process control algorithm such as nitrate concentration and pH [7,8]. Catalytic hydrogenation of nitrate to nitrogen with H_2 as electron donor over solid catalysts is another option. Yoshinaga et al. has showed that a catalyst, Pd–Cu supported on active carbon, could yield 75% of N_2 during nitrate reduction by hydrogenation [8]. However, catalytic reduction by hydrogen is not suitable for large scale application. Also, this method requires continuous feeding of H_2 [9–12]. Therefore, electrochemical reduction method becomes an alternative for overcoming the limitations of biological denitrification and catalytic hydrogenation. Electrochemical reduction on solid electrodes offers a promising approach to remove nitrate from water because of its high treatment efficiency, lack of sludge production, and relatively low investment costs [13–19]. Li et al. have showed that nitrate can be successfully reduced and converted to N_2 by electrochemical reduction over a Cu–Zn cathode and a Ti/IrO_2–Pt anode [20]. Also, de Vooys et al. have demonstrated that the conversion from nitrate to N_2 can be controlled by Cu loading on the Pd–Cu electrode [21]. Although electrochemical reduction of nitrate to N_2 has been widely studied, the mechanism still remains relatively unknown due to high reactivity and instability of nitrate reduction products. Moreover, in most cases, nitrate has been converted to unwanted byproducts such as nitrite and ammonia, which are toxic to many aquatic lives. To improve the selectivity of nitrate reduction toward N_2, a wide variety of cathodic metals and alloys, such as Pb [22,23], Ni [22,24,25], Fe [22], Cu [21,26–28], Pt [24,29–31], Zn [23], Ru [31], Pd [21,31,32], C [19,22], and Ir [29,31], Pt-Ir [29], Pd-Cu [8,12,21] have been studied. Among these materials, Cu was the most studied due to its high selectivity and efficiency [26] for the conversion of nitrate into nitrite, which has been reported to be the rate-determining step in the nitrate reduction mechanism [31]. However, nitrate reduction on Cu electrode mainly leads to

* Corresponding author. Fax: +1 302 831 3640.
E-mail address: huang@udel.edu (C.P. Huang).

http://dx.doi.org/10.1016/j.apcatb.2015.06.028
0926-3373/

the formation of nitrite and ammonia [26,33]. Vorlop and Tacke [12] were the first to report that a second metal, Pd, in addition to Cu could improve the N_2 selectivity during the electrochemical reduction of nitrate. Cu exhibits a catalytic effect that restricts the adsorption of hydrogen on the cathode surface thereby enhancing the adsorption of nitrate [34]. After the adsorption of nitrate, Cu has a negative influence both on the activity and selectivity of nitrite reduction towards N_2. Both de Vooys et al. [21] and Ghodbane et al. [14] have reported that nitrogen generation increases with increasing amount of Pd on the electrode surface; that is, Pd gives high reactivity on nitrite reduction.

Many have reported electrochemical nitrate reduction using various metal electrodes, but only a few have discussed the effect of applied potential on the nitrate reduction products. Ryter et al. [33] reported that the nitrate electroreduction process was strongly dependent on the applied potential. For example, nitrate was reduced to nitrite at −0.9 V (vs. Hg/HgO) but was reduced to hydroxylamine at −1.1 V (vs. Hg/HgO) using Cu electrode. Their results demonstrated that an optimum applied potential was important to effective nitrate conversion in order to avoid the formation of unwanted byproducts and additional post-treatment of the finished water.

The objective of this study was to determine the effect of applied potential and electrode material on nitrate reduction and its byproducts. The cyclic voltammetric curve was convoluted to establish the potential corresponding to the individual half redox reaction. Additionally, the electrode materials were characterized via X-ray diffraction (XRD) and scanning electron microscope (SEM) as to assess the effect of electrode material on nitrate reduction.

2. Experimental

2.1. Materials

Sodium nitrate, sodium nitrite, sodium carbonate were obtained from Fisher Scientific, Pittsburgh, PA, USA and were of certified grade according to American Chemical Society (ACS). Sodium perchlorate (purity >98%) and sodium bicarbonate (purity >99.7%) were purchased from ACROS, Fair Lawn, NJ, USA. Sodium hydroxide (purity >97.0%) and methanesulfonic acid were purchased from Sigma–Aldrich, St Luis, MO USA. Deionized water was treated with Mega-Pure System (Model MP-290). Platinum wire (Fisher Scientific, 1284987, od: 0.5 mm) was purchased from Fisher Scientific, Pittsburgh, PA, USA. Stainless steel mesh (corrosion-resistant 304 stainless steel woven wire cloth, 100 × 100 mesh, or 0.0045" wire diameter) was obtained from McMaster-Carr Co., Elmhurst, IL, USA. For catalytic material preparation, cupric sulfate (purity >99%), and palladium chloride (purity >98%) were purchased from Sigma–Aldrich, St Luis, MO, USA.

2.2. Electrode preparation

The raw stainless steel mesh was cut into small pieces (ca. 5 cm × 10 cm) and washed in detergent solution. After cleaning, the mesh was rinsed with deionized water and dried in a dryer for 1 h. The metal ion solutions were prepared by dissolving an appropriate amount of cupric sulfate and palladium chloride in deionized water at concentration range of 0.01 and 0.1 M, respectively. All electrodeposition experiments were carried out at room temperature by using a two-electrode system, which was connected to a potentiostat (Model WP705B, Vector-VID) [35]. The washed stainless steel mesh was used as working electrode and graphite was selected as the counter electrode. Both electrodes were immersed in the metal ion solution in a 250-mL beaker. Cu metal deposition process was performed at constant current of 0.3 A for 5 min, and then current was increased to 0.6 A for additional 3 min at each side. Pd metal deposition process was operated at constant current of 0.3 A for 1.5 min and then the current was increased to 0.6 A for 1.5 min at each side. After deposition, the metal coated stainless steel mesh was washed with deionized water and dried under ambient environment. The electrodeposited Pd–Cu composition was calculated from the Faraday's laws. The Pd–Cu electrode so fabricated had a Pd weight fraction of 0.4. Note that in order to avoid overloading the instrument during cyclic voltammetric runs, the electrodes were cut into small pieces as to minimize the current output.

2.3. Voltammetry experiments

All experiments were carried out in a three-electrode system at room temperature. The three electrodes were connected to a potentiostat (model AFRDE 4, Pine Instrument Inc., USA), which controlled the applied voltage and recorded corresponding current. The stainless steel supported Cu (Cu/SS) or Pd–Cu (Pd–Cu/SS) electrode was the working electrode. A platinum wire and a saturated calomel electrode (SCE) were the counter electrode and the reference electrode, respectively. The reaction vessel was a 500-mL glass beaker. $NaClO_4$ solution at a concentration of 0.05 M was the electrolyte. The pH value during electrolysis experiment was controlled by the $NaHCO_3$–Na_2CO_3 buffer. Voltammetry experiments were operated at a sweep rate of 10 mV/s between −1.0 V and 0.6 V (vs. SCE) to evaluate the activity of the electrode in nitrate reduction. In all cases, the voltammetric experiment was scanned 5 times in the above potential range to achieve a stable voltammogramm.

2.4. Analytical methods

Nitrate and nitrite were measured by a Dionex ion chromatograph (IC) system equipped with a GP50 pump, ED 40 conductance detector, Dionex IonPac AC20 column (4 mm × 250 mm.), and Dionex AS 40 automatic sampler. The effluent mobile phase was a mixture of deionized water and 50 mM NaOH and the injection volume was 25 μL, which yielded a flow rate of 1 mL/min. At different time intervals, 3 mL of sample were withdrawn from the electrochemical cell for chemical analysis. A Dionex ion chromatograph (IC) system equipped with a GP40 pump, CD 20 conductance detector, Dionex IonPac CS16 column (0.5 mm × 250 mm.), and Dionex AS 3500 automatic sampler was used to measure the ammonium concentration. The effluent mobile phase was a mixture of deionized water and 0.1 M methanesulfonic acid and the injection volume was 25 μL, which delivered a flow rate of 1 mL/min. The concentration of nitrogen gaseous species was quantified by mass-balance.

2.5. Surface characterization

The crystallinity of Cu and Pd–Cu catalysts were identified by X-ray diffraction (XRD, Rigaku D-Max B) with Cu Kα radiation. Each sample was operated at 30 kV beam voltage and 30 mA current, and scanned between 30° and 90° at a scan rate of 0.6 (deg/min). The elements and crystal structures were characterized by matching the XRD pattern of each sample against library data (JCPDS, PDF no. 85-1326). Surface morphology and structure of the deposits were investigated by a scanning electron microscopy (SEM, JSM 7400F) at an accelerating voltage of 3 kV. The composition of each sample was determined by X-ray photoelectron spectroscopy (XPS, Omicron EA125). Non-monochromatic Al X-rays (1486.5 eV) were employed. CasaXPS software was used to convolute the peaks. C 1s peak related to the C—C bond located at 284.6 eV was used as a reference peak for calibration.

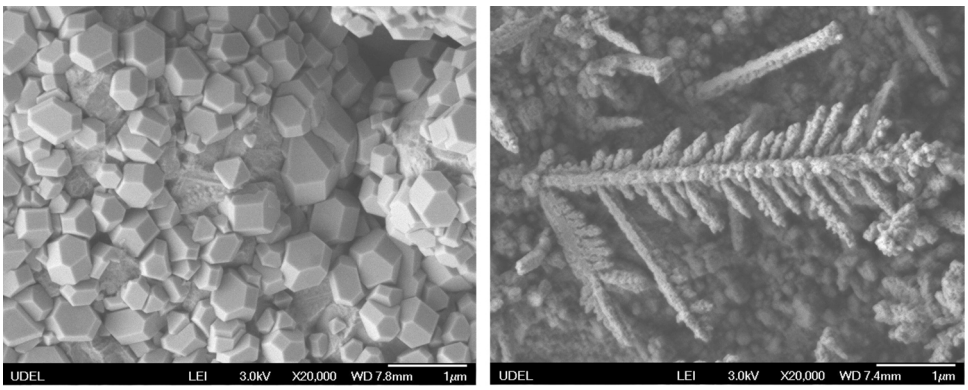

Fig. 1. SEM images of the surface of (a) the Cu/SS electrode and (b) the Pd–Cu/SS electrode.

3. Results and discussion

3.1. Electrode (Cu/SS, Pd–Cu/SS) characterization

Fig. 1a and b show the SEM images of the Cu and Pd–Cu electrode surfaces, respectively. As presented in Fig. 1a and b, all electrodeposited materials uniformly covered the stainless steel substrate. Also, it can be noted that these two electrodes exhibited distinct surface morphologies. Since the Cu/SS and the Pd–Cu/SS electrode were synthesized under same experimental conditions, the difference in the surface morphology very likely was due to the presence of Pd. Therefore, it is believed that Pd must be incorporate into the Cu/SS electrode and bring about structural changes. Fig. 1a shows the polyhedral feature in the Cu/SS electrode with smooth crystal planes. The average diameter of the large copper crystals was approximately 0.6 μm and that of the smaller crystals was 0.3 μm calculated according to the Scherrer equation. The SEM micrographs of the Cu/SS electrode was identical to that reported by Zhang et al. [36], which confirmed its successful preparation. Moreover, the surface of the Pd–Cu/SS electrode (Fig. 1b) appeared relatively rough and formed dendrites, which was similar to those reported by Löffler et al. [37].

Fig. 2 shows the XRD pattern of the Cu/SS and Pd–Cu/SS electrodes, respectively. It can be observed that the Cu/SS electrode (Fig. 2a) illustrates sharp peaks at $2\theta = 43.35$, 50.46, and 74.23, which are consistent with the values reported by Yashinaga el al. [8]. However, no Pd peaks were detected for the Pd–Cu/SS electrode (Fig. 2b). It is hypothesized that there was formation of Cu_3Pd phase on the electrode surface. According to Yoshinaga et al., the Cu_3Pd phase has two strong peaks at $2\theta = 42$ and 48 in XRD pattern, which are very close to Cu peaks. (Note: The two minor peaks of Cu_3Pd phase at $2\theta = 68$ and 82 were probably covered by the background noise). Thus, the peaks of Cu and Cu_3Pd crystallites might be overlapped with each other in the XRD pattern as shown in Fig. 2b. Löffler et al. [37] also reported a similar Cu_3Pd dendrites, which supported our assertion of Cu_3Pd formation on the Pd–Cu/SS electrode.

In order to investigate the oxidation state of Cu and Pd on the electrode surface, XPS was applied to characterize the chemical state of elements on the electrode. Fig. 3 represents the XPS high resolution scan for Cu 2p on the surface of the Cu/SS and the Pd–Cu/SS electrodes. For both electrode surfaces, the binding energy of Cu 2p3/2 (931.9 eV) and Cu 2p1/2 (951.7 eV) were consistent with that reported by Liu el al. [38]. The Cu 2p region was composed of three identical peaks at 931.2, 934.3, and 941.4 eV, individually, which were identified as Cu(0), Cu_2O, and CuO, respectively [39]. Note that the Pd 3d peaks were not captured under our XPS scan because of the combination of low Pd concentration on the electrode surface and instrument resolution.

3.2. Scan rate selection

Fig. 4a shows the voltammetric curve of the solution containing 0.6 mM of $NaNO_3$ in 0.01 M of $NaClO_4$ electrolyte over the Cu/SS electrode as a function of scan rate. The voltammetric curves were measured in the potential range from −1.0 V to 0.6 V (vs. SCE). A reduction peak was observed while sweeping in the negative direction under all scan rates and there was no corresponding

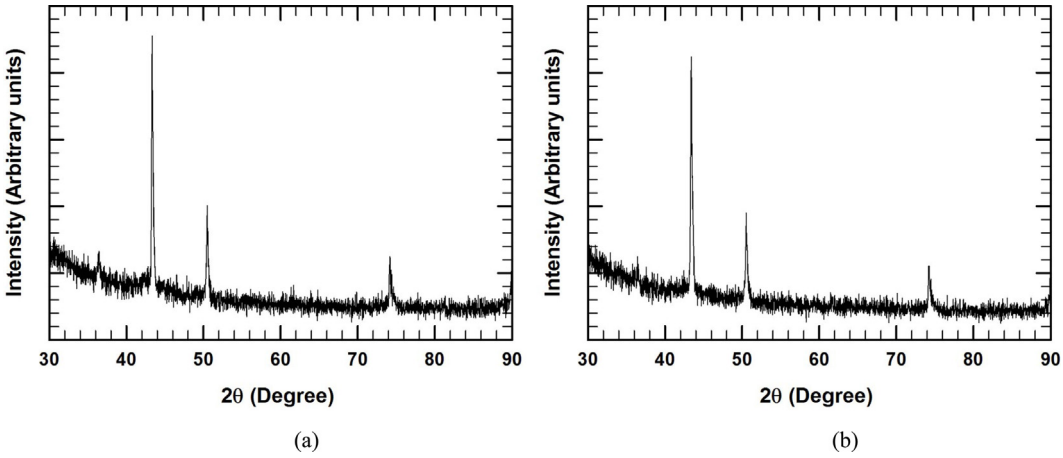

Fig. 2. XRD patterns of (a) the Cu/SS electrode and (b) the Pd–Cu/SS electrode.

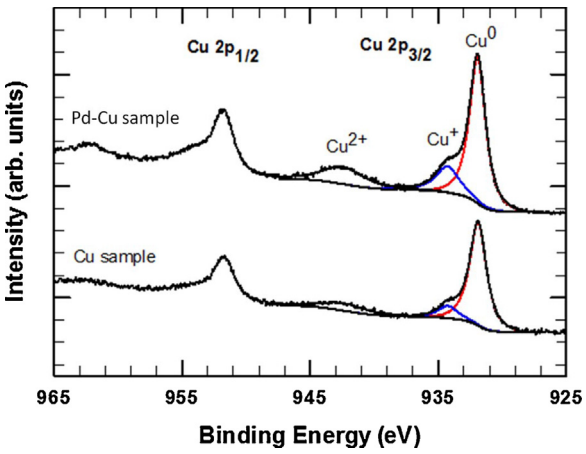

Fig. 3. XPS spectra of the Cu/SS and the Pd–Cu/SS electrodes.

oxidation peak under positive scan, indicating the presence of an irreversible redox reaction. In addition, it was noted that the reduction peak was shifted to more negative potential as the scan rate was increased. The result was consistent with an irreversible system. For an irreversible process, the peak potential is a function of the scan rate, shifting (for a reduction) in the negative direction with increase in scan rate as described in Eq. (1) [40].

$$E_p = E^0 - \frac{RT}{\alpha F}\left[0.78 + \ln\left[\frac{D^{1/2}}{k^0}\right] + \ln\left[\frac{\alpha F V}{RT}\right]^{1/2}\right] \quad (1)$$

where E_p is the peak potential (V), E^0 is the formal potential of an electrode (V), R is the gas law constant (8314 J mol^{-1} K^{-1}), T is the temperature (K), F is the Faraday constant (96,485 Ceq^{-1}), α is the transfer coefficient, D is the diffusion coefficient (2×10^{-5} cm^2 s^{-1} in this case of nitrate), k^0 is the standard rate constant (cm s^{-1}), and V is the potential scan rate (V s^{-1}).

The magnitude of the peak current in the C–V curve can be expressed by the Nicholson and Shain equation [41–43], i.e.,

$$I_p = -\left(2.99 \times 10^5\right) n(\alpha)^{0.5} A D^{0.5} V^{0.5} C \quad (2)$$

where I_p is the cathodic peak current (A), n is the number of electron involved in the reaction, α is the transfer coefficient, A is the electrode surface area (cm^2), D is the nitrate diffusion coefficient (2×10^{-5} cm^2 s^{-1}), V is the potential scan rate (V s^{-1}), and C is the bulk nitrate concentration (mol cm^{-3}).

Fig. 4b is a plot of the reduction peak current, I_p, vs. the square root of scan rate, $V^{1/2}$, where the Cu/SS electrode surface area, A, was 1.5 cm^2. There were two slopes of the plot and both of them exhibited a linear relationship (R^2 = 1.00 and 0.98, respectively) between I_p, and $V^{1/2}$, meaning that the result did obey the Nicholson and Shain equation (Eq. (2)). Also, these two slopes suggested two separate reduction steps occurred at the reduction peak around −0.15 V (vs. SCE). In Fig 4a, it can be noted that the signal of reduction peak is more pronounced (steeper) at lower scan rate. Both scan rates of 5 mV s^{-1} and 10 mV s^{-1} could yield sufficient resolution in current measurements, but a scan rate of 10 mV s^{-1} was selected in all voltammetric experiments for the sake of time-saving.

3.3. Polyhedron-pattern Cu/SS electrode

Fig. 5a shows the voltammetric curve at a Cu/SS electrode starting from 0.5 V toward −0.8 V (vs. SCE) at the scan rate of 10 mV/s in 0.05 M of $NaClO_4$ electrolyte with and without NO_3^- addition. When the NO_3^- concentration was increased, more cathodic peaks appeared as shown in Fig. 5a. The formation of cathodic peaks was resulted from the reduction of products during negative (cathodic) scan. To resolve multiple peaks in the reduction curve, Origin 8.0 Pro software was applied to fit the data. Fig. 5b shows the fitting result of 35 mM NO_3^- solution. Four reduction peaks (vs. SCE) were identified at −0.096 V (R_1), −0.202 V (R_2), −0.283 V (R_3), and −0.400 V (R_4), respectively. To determine the corresponding redox couple for each peak, the number of electron transfer at each peak was calculated via the Nicholson–Shain equation (Eq. (2)). The term α in Eq. (2) was obtained from the following relationship [42]:

$$|E_p - E_{p/2}| = \frac{47.7}{\alpha} \quad (3)$$

where E_p is the peak potential (mV) and $E_{p/2}$ is the half-peak potential (mV), located at the point where the current is half of the peak value. Therefore, the current of cathodic peaks I_p can be plotted as a function of bulk nitrate concentration, C, as shown in Fig. 5c, where the Cu/SS electrode surface area, A, was 0.09 cm^2. The peak current and the bulk nitrate concentration exhibited a linear relationship in all cases (i.e., R_1–R_4), and the slope can be used to calculate the number of electrons transferred, n, during the reaction. From the results (i.e., C = 6, 15, 20, 25, 30, and 35 mM), the n value for R_1 peak was 1, meaning that the R_1 peak was corresponding to a one-electron transfer redox reaction. The number of electron transfer for R_2–R_4 peaks were calculated in the same fashion. The n value for R_2 peak was equal to 1. The n value for R_3 and R_4, calculated from the three reduction curves at high concentration (C = 25, 30, and 35 mM), was

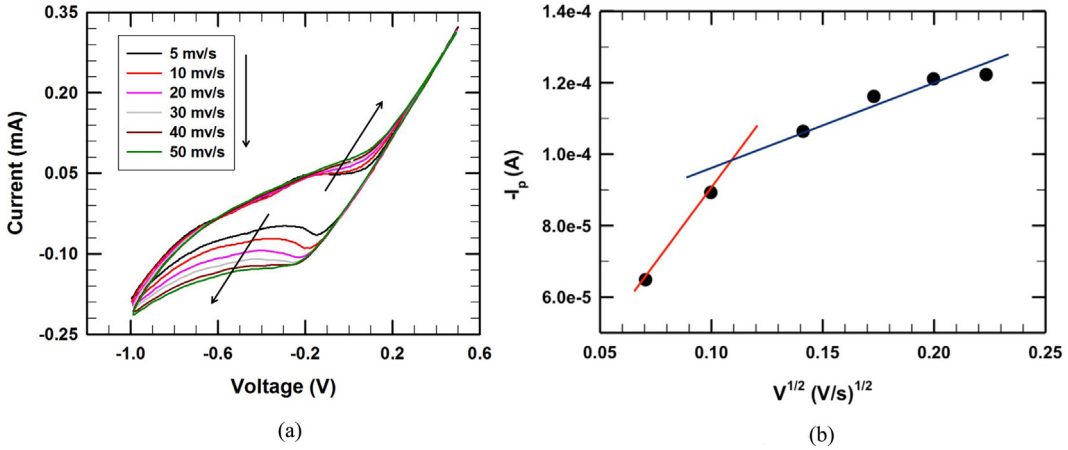

(a) (b)

Fig. 4. (a) Cycle voltammetric curves for the Cu/SS electrode recorded at different scan rate (from 5 to 50 mV/s) of 0.6 mM of $NaNO_3$ solution in the presence of 0.01 M of $NaClO_4$ electrolyte. (b) The peak currents vs. the square root of the scan rate ($V_{1/2}$) extracted from cycle voltammetric curves shown in (a).

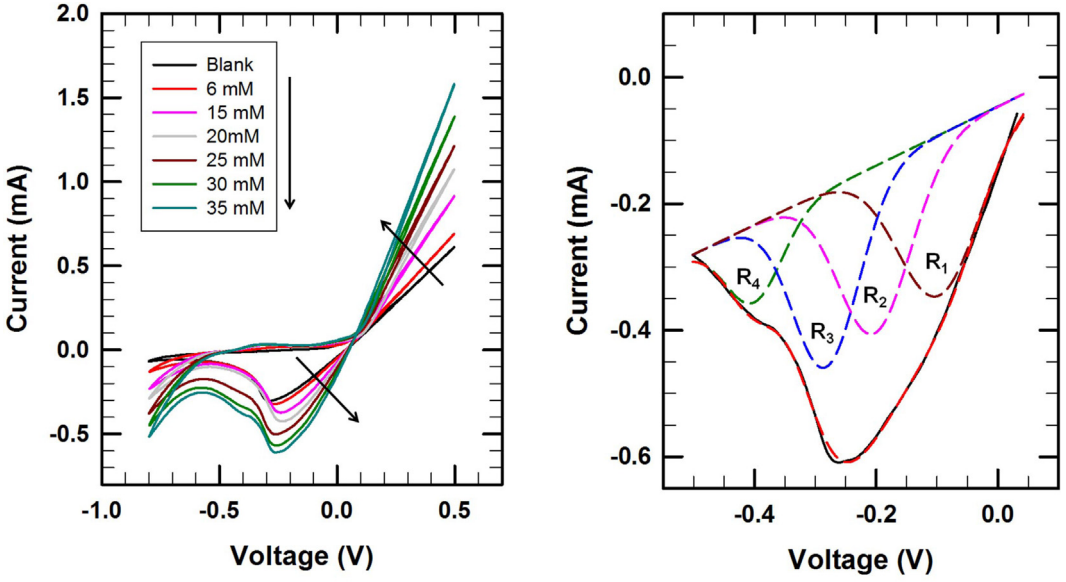

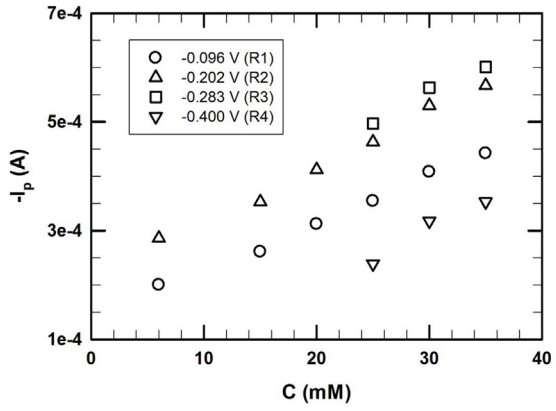

Fig. 5. (a) Cycle voltammetric curves scanned at the rate of 10 mV/s on the Cu/SS electrode with different nitrate concentrations (from 6 to 35 mM) in 0.05 M of $NaClO_4$ electrolyte solution (i.e., blank). (b) The fitting results from the cycle voltammetric curve of 35 mM of $NaNO_3$ solution (a) on the Cu/SS electrode. (c) The corresponding Nicholson and Shain plot at R_1–R_4 peaks.

2, and 3, respectively. Table 1 lists the slope, α, and n values for all peaks. The α value decreased with increase in peak potential due to nitrate reduction that was favored under high reduction potential. Generally, α is a potential-dependent factor and can be used to estimate the symmetry of the energy barrier. If the redox reaction is in equilibrium, α would be equal to 0.5. At $0 < \alpha < 0.5$ and $0.5 < \alpha < 1$, the reduction (cathodic) and the oxidation (anodic) was favored, respectively, [40], which was in agreement with our results.

Theoretically, there were eight reduction peaks, i.e., eight electrons transferred, during voltammetric scan of the nitrate solution. However, only seven electron transfers were detected in the present study. In order to identify the individual catholic peak and assign a peak to the corresponding reduction reaction, more experiments must be conducted as to reveal the mechanisms of nitrate reduction.

Table 1
Electrochemical parameters (slope, α, and n) of nitrate reduction on Cu/SS electrode.

Peak ID	−0.096 V (R_1)	−0.202 V (R_2)	−0.283 V (R_3)	−0.400 V (R_4)
Slope	9×10^{-6}	10^{-5}	10^{-5}	10^{-5}
$n\alpha^{1/2}$	0.75	0.83	0.83	0.83
α	0.56	0.35	0.23	0.10
n	1	1	2	3

To distinguish the nitrate and the nitrite reduction peaks on the Cu/SS electrode, a similar experiment using nitrite solution at various concentrations was conducted as shown in Fig. 6a. It can be seen that the cathodic peaks from the electrochemical reduction of nitrite appeared at the applied potential below −0.28 V (vs. SCE), which indicated that the reduction peaks (R_1, R_2) at −0.096 V and −0.202 V (vs. SCE) in nitrate reaction was corresponding to the following nitrate-to-nitrogen dioxide and nitrogen dioxide-to-nitrite reduction, respectively, i.e.,

$$NO_3^- + e^- + H_2O = NO_2 + 2OH^- \quad (4)$$

$$NO_2 + e^- = NO_2^- \quad (5)$$

Additionally, there were significant changes for the nitrite reduction waves at elevated concentrations, which demonstrated that the reduction wave included multiple peaks, meaning nitrite reduction contained several steps. Fig. 6b shows the fitting result of 35 mM NO_2^- solution. Three reduction peaks (vs. SCE) were obtained at −0.290 V (P_1), −0.387 V (P_2), and −0.453 V (P_3), respectively. Based on the Nicholson–Shain equation (Eq. (2)), a plot of

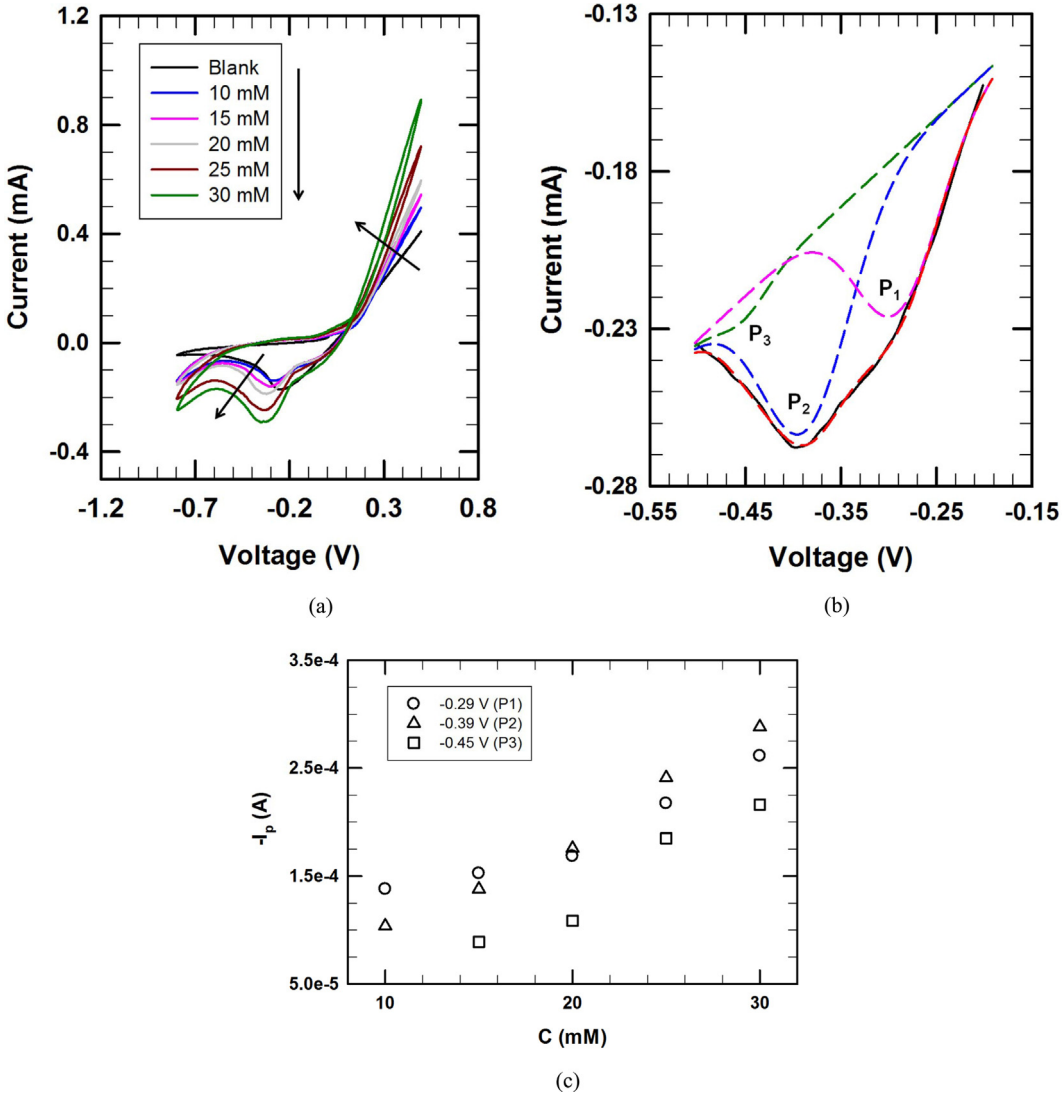

Fig. 6. (a) Cycle voltammetric curves scanned at the rate of 10 mV/s on the Cu/SS electrode with different nitrite concentrations (from 10 to 35 mM) in 0.05 M of $NaClO_4$ electrolyte solution (i.e., blank). (b) The fitting Results from the cycle voltammetric curve of 35 mM of $NaNO_2$ solution (a) on the Cu/SS electrode. (c) The corresponding Nicholson and Shain plot at P_1–P_3 peaks.

the P_1, P_2, and P_3 peak current, I_p, as a function of bulk nitrite concentration was constructed as shown in Fig. 6c, where the Cu/SS electrode surface area, A, was 0.09 cm^2. The plot yielded three straight lines, which slope was used to estimate the number of electrons involved in the redox reaction associated with the P_1, P_2, and P_3 peak, individually. The n value was 1, 2, and 2 for peak P_1 P_2, and P_3, respectively, as determined from five nitrate concentrations studied (i.e., C = 10, 15, 20, 25, and 30 mM). Table 2 lists the slope value, α, and n calculated as shown in Fig. 6c. As mentioned above, the increase in reduction potential caused a decrease in α. To understand the corresponding redox reactions at all peaks in nitrate reduction, the voltammetric curve from nitrite and nitrate reduction at concentration of 35 mM as shown in Figs. 5 and 6b were compared and analyzed. It can be noted that the P_3 peak was located at the leftmost position during nitrite reduction reaction, which indicated the production of ammonia at −0.453 V. Therefore, R_3 peak was assigned to the reduction of nitrite into nitrous oxide via the reaction:

$$2NO_2^- + 4e^- + 3H_2O = N_2O + 6OH^- \quad (6)$$

R_4 peak was assigned to the reduction of nitrous oxide to hydrazine via the reaction:

$$N_2O + 6e^- + 5H_2O = N_2H_4 + 6OH^- \quad (7)$$

Also, according to the n value for the P_1, P_2 and P_3 peak, P_1 peak could be assigned to the reduction of nitric oxide into nitrous oxide via the reaction:

$$2NO + 2e^- + H_2O = N_2O + 2OH^- \quad (8)$$

P_2 peak was assigned to the reduction of nitrous oxide to hydroxylamine via the reaction:

$$N_2O + 4e^- + 5H_2O = 2NH_2OH + 4OH^- \quad (9)$$

Table 2
Electrochemical parameters (slope, α, and n) of nitrite reduction on Cu/SS electrode.

Peak ID	−0.290 V ($P1$)	−0.387 V ($P2$)	−0.453 V ($P3$)
Slope	6×10^{-6}	9×10^{-6}	9×10^{-6}
$n\alpha^{1/2}$	0.50	0.75	0.75
α	0.22	0.19	0.13
n	1	2	2

Table 3
Electrochemical parameters (slope, α, and n) of nitrate reduction on Pd–Cu/SS electrode.

Peak ID	−0.017 V (Q_1)	−0.123 V (Q_2)	−0.197 V (Q_3)	−0.296 V (Q_4)	−0.411 V (Q_5)
Slope	5×10^{-6}	3×10^{-6}	5×10^{-6}	8×10^{-6}	10^{-5}
$n\alpha^{1/2}$	0.63	0.38	0.63	1.00	1.25
α	0.98	0. 35	0.30	0.24	0.17
n	1	1	1	2	3

P_3 peak was assigned to the reduction of hydroxylamine into ammonia via the reaction:

$$NH_2OH + 2e^- + 2H_2O = NH_4^+ + 3OH^- \quad (10)$$

According to the above results, the nitrate reduction process can be described at various reduction potentials on copper electrode. Results clearly indicated that the nitrate reduction process was significantly governed by the reduction potential.

3.4. Pd–Cu/SS alloy dendrite electrode

As mentioned above (in Section 1), the electrode material is one of the key factors governing electrochemical reaction. Recently, copper has been proved to be the best material for the electrocatalytic reduction of nitrate compared to other materials such as nickel, graphite, and platinum [26]. However, electrochemical nitrate reduction over pure copper electrode usually led to the formation of nitrite and ammonia, which are toxic [43]. Bimetallic, palladium-copper, electrode with the maximum N_2 selectivity of 60–70% has been reported [14,21]. It is conceivable that palladium favors the reduction of nitrite to nitrogen. However, to the best of our knowledge, there is no report about the effect of palladium-copper electrode on the applied potential and reduction process in nitrate solution. Experiment on nitrate reduction over Pd–Cu/SS electrode was conducted in seven nitrate concentrations (i.e., C = 6, 15, 20, 25, 30, 35, and 40 mM). Fig. 7a shows the voltammetric curve of nitrate on Pd–Cu/SS electrode, as a function of nitrate concentration. The nitrate reduction peaks were increased with increase in nitrate concentration, which was in agreement with results on nitrate reduction over Cu/SS electrode. The reduction of NO_3^- solution at 35 mM on the Pd–Cu/SS electrode was fitted in the same fashion as described above with Origin Pro as shown in Fig. 7b. Five reduction peaks (vs. SEC) were obtained at −0.017 V (Q_1), −.123 V (Q_2), −0.197 V (Q_3), −0.296 V (Q_4), and −0.411 V (Q_5), respectively. The number of electron transfer at individual peak was calculated via the Nicholson–Shain equation (Eq. (2)) from the peak current and the bulk nitrate concentration for all peaks (i.e., Q_1–Q_5) as shown in Fig. 7c, where the Pd–Cu/SS electrode surface area, A, was 0.06 cm^2. The n value at Q_1, Q_2, Q_3 Q_4, Q_5, and Q_6 peak were l, 1, 1, 2, and 3, respectively. The value of slope, α, and n in all cases were determined as shown in Fig. 7c and summarized in Table 3. As mentioned above, a decrease in α value was due to an increase in reduction potential. In this study, nitrate reduction on the Pd–Cu/SS electrode exhibited eight electrons transfer, indicating the final product of nitrate reduction will be ammonia. Thus, the following assignment of the peaks can be suggested: Q_1 from direct nitrate reduction to nitrogen dioxide (Eq. (4)); Q_2 from nitrogen dioxide reduction to nitrite (Eq. (5)); Q_3 from nitrite reduction to nitric oxide (Eq. (11)); Q_4 from nitric oxide reduction to nitrogen gas (Eq. (12)); and Q_5 from nitrogen gas reduction to ammonia (Eq. (13)):

$$NO_2^- + e^- + H_2O = NO + 2OH^- \quad (11)$$

$$2NO + 4e^- + 2H_2O = N_2 + 4OH^- \quad (12)$$

$$N_2 + 6e^- + 8H_2O = 2NH_4^+ + 8OH^- \quad (13)$$

Table 4
The potentials of nitrate reduction with respect to the formation of products on Cu/SS electrode.

Redox reaction	E_p (V)[a]	E_p (V)[b]	Peak ID
$NO_3^- + e^- + H_2O = NO_2 + 2OH^-$	−0.096	0.145	R_1
$NO_2 + e^- = NO_2^-$	−0.202	0.039	R_2
$2NO_2^- + 4e^- + 3H_2O = N_2O + 6OH^-$	−0.283	−0.042	R_3
$2NO + 2e^- + H_2O = N_2O + 2OH^-$	−0.290	−0.049	P_1
$N_2O + 4e^- + 5H_2O = 2NH_2OH + 4OH^-$	−0.387	−0.146	P_2
$N_2O + 6e^- + 5H_2O = N_2H_4 + 6OH^-$	−0.400	−0.159	R_4
$NH_2OH + 2e^- + 2H_2O = NH_4^+ + 3OH^-$	−0.453	−0.212	P_3

[a] : vs. SCE.
[b] : vs. NHE.

The nitrate reduction steps changed when using the Pd–Cu/SS electrode (Eqs. (11)–(13) vs. Eqs. (6) and (7)). Interestingly, it must be mentioned that the Pd–Cu/SS electrode was found to promote N_2 selectivity. The result was likely due to the surface coverage of N-species, namely N* and NO*, on Pd monometallic sites as reported by De Vooys et al. [21]. Additionally, the reduction potential at each peak, namely, Q_1–Q_5 underwent a positive (anodic) shift of 0.079 V (vs. SCE) on the Pd–Cu/SS electrode compared to the Cu/SS electrode because of the change of electronic structure of Cu in the presence of Pd [44].

The cathodic current (Fig. 5b) contributed from nitrate to nitrite (R_1 and R_2) on the Cu/SS electrode was about six times larger than that of the similar reaction (Fig. 7c, Q_1 and Q_2) on the Pd–Cu/SS electrode. As the copper was covered by the palladium in the Pd–Cu/SS electrode, there was a significant change of the cathodic current due to the presence of active copper sites. Prusse et al. reported that the role of copper in the Pd–Cu catalyst was to enhance the reduction of nitrate to nitrite and the role of palladium in the Cu-Pd catalyst was to further reduce nitrite to other products [26,31,45]. Our results were in agreement with that of Prusse et al. [26,31,45]. Hence, it further demonstrates the importance of electrode material in nitrate reduction. Additionally, the applied potential can control the mode of nitrate reduction on the Cu-Pd/SS electrode as well as on the Cu/SS electrode.

3.5. The relationship between reduction potential and reaction product

Table 4 summarizes the potential of nitrate reduction with respect to the formation of products on the Cu/SS electrode. Based on results shown in Figs. 5 and Fig. 6b, the reduction potential of nitrite-to-nitric oxide could be calculated from the P_1 peak (nitric oxide-to-nitrous oxide) and R_3 peak (nitrite to nitrous oxide) using Gibbs free energy. A similar method was applied to calculate the reduction potential of the hydroxylamine-to-hydrazine (using R_4 and P_2) and hydrazine-to-ammonia (using P_3 and hydroxylamine-to-hydrazine). The nitrate reduction potential on Cu/SS electrode can be summarized as the following: $NO_3^- \xrightarrow{-0.096V(R_1)} NO_2 \xrightarrow{-0.202V(R_2)} NO_2^- \xrightarrow{-0.276V(R_3,P_1)} NO \xrightarrow{-0.290V(P_1)} N_2O \xrightarrow{-0.387V(P_2)} NH_2OH \xrightarrow{-0.426V(P_2,R_4)} N_2H_4 \xrightarrow{-0.480V(P_3,-0.426V)} NH_4^+$

Table 5 lists the reduction potential of nitrate with respect to different products on the Pd–Cu/SS electrode. In summary, the results demonstrated that the electrode material played a great role on the

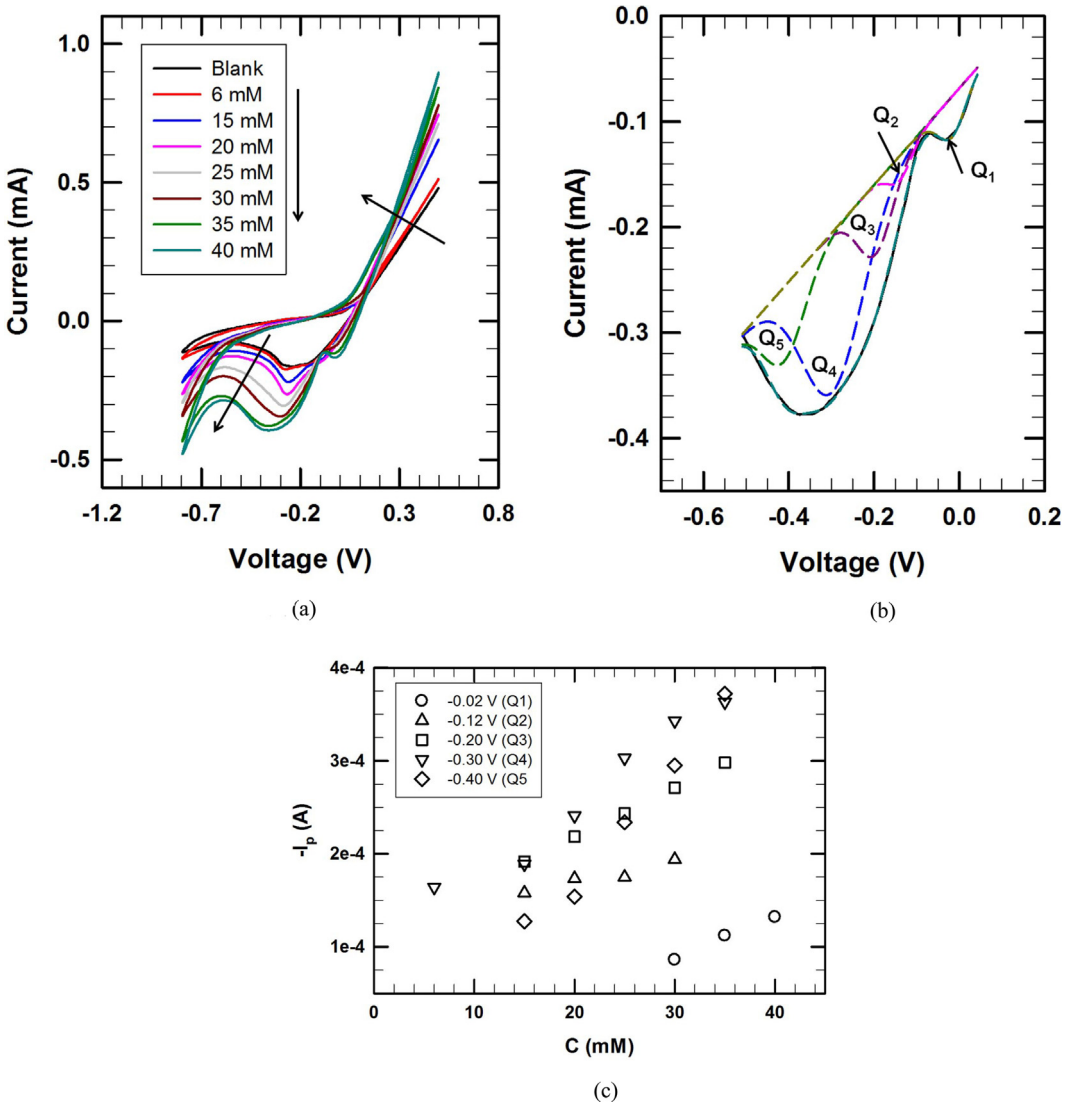

Fig. 7. (a) Cycle voltammetric curves scanned at the rate of 10 mV/s on the Pd–Cu/SS electrode with different nitrate concentrations (from 6 to 40 mM) in 0.05 M of $NaClO_4$ electrolyte solution (i.e., blank). (b) The fitting results from cycle voltammetric curve of 35 mM of $NaNO_3$ solution (a) on the Pd–Cu/SS electrode. (c) The corresponding Nicholson and Shain plot at Q_1–Q_5 peaks.

total reaction scheme (which was consisted of several steps) and affected the reaction rate and the selectivity of reaction products. Table 6 summarizes the nitrate reduction potential for nitrate-to-nitrite, and nitrite-to-hydroxylamine reaction together with of Ryter et al. [33]. Results showed that the nitrate reduction potential obtained from the present study was in agreement with that reported by Ryter et al. [33].

Table 5
The potentials of nitrate reduction with respect to the formation of products on Pd–Cu/SS.

Redox reaction	E_p (V)[a]	E_p (V)[b]	Peak ID
$NO_3^- + e^- + H_2O = NO_2 + 2OH^-$	−0.017	0.224	Q_1
$NO_2 + e^- = NO_2^-$	−0.123	0.118	Q_2
$NO_2^- + e^- + H_2O = NO + 2OH^-$	−0.197	0.044	Q_3
$2NO + 4e^- + 2H_2O = N_2 + 4OH^-$	−0.296	−0.055	Q_4
$N_2 + 6e^- + 8H_2O = 2NH_4^+ + 8OH^-$	−0.411	−0.170	Q_5

[a] : vs. SCE.
[b] : vs. NHE.

3.6. Nitrate reduction at different applied potentials on the Pd–Cu/SS electrode

Applied potential is a powerful parameter for controlling the rate and mode of electrochemical reactions. To identify the relationship between the applied potential and the selectivity of nitrate reduction products, the influence of applied potential on the yield of different products was studied by the reduction of nitrate on the Pd-Cu/SS electrode at different potentials ranging from −0.1 to −0.3 V (vs. SCE). Fig. 8a shows the concentration change as a function of reaction time at the applied potential of -0.1 V (vs. SCE). Nitrate, nitrite, and ammonium were detected in the liquid phase

Table 6
The reduction potentials of nitrate-to-nitrite, and nitrite-to-hydroxylamine from our study and literature [33].

Reaction	E_p (V)[a]	E_p (V)[b]
$NO_3^- + 2e^- + H_2O = NO_2^- + 2OH^-$	−0.165	−0.150
$NO_2^- + 4e^- + 4H_2O = NH_2OH + 5OH^-$	−0.365	−0.335

[a] : vs. SCE (Ryter et al.; room temperature).
[b] : vs. SCE (our study; room temperature).

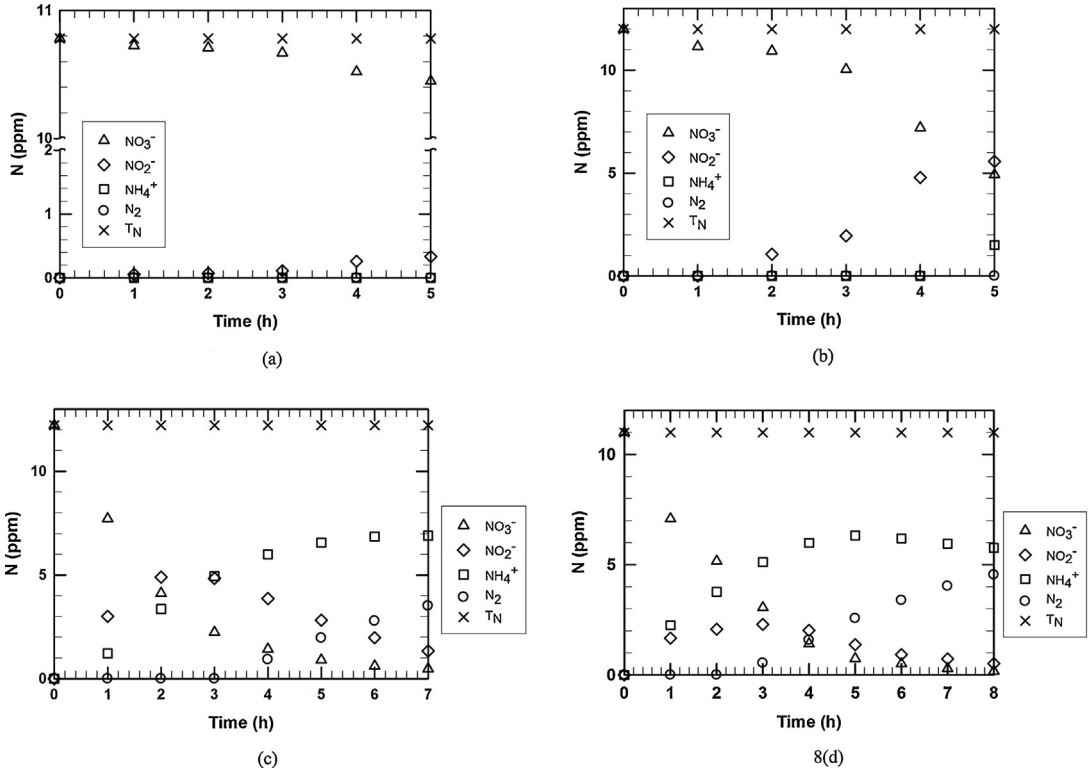

Fig. 8. Variation of nitrate, nitrite, nitrogen gas and ammonia (in unit of ppm as N) at the reduction potential of (a) −0.1 V, (b) −0.2 V, (c) −0.23 V, and (d) −0.3 V solution containing 0.01 M of $NaClO_4$ electrolyte and 0.6 mM of $NaNO_3$ on the Pd–Cu/SS electrode.

while the gaseous products were calculated via mass-balance. It was clear that the only product formed at -0.1 V (vs. SCE) was nitrite, 3% nitrate was reduced to nitrite in accordance with the voltammetric results showed in Fig. 7b.

At −0.2 V (vs. SCE) (Fig. 8b), nitrate was reduced to yield 59 % nitrite and 6% ammonium. According to the reduction potential shown in Eq. (11), nitrogen dioxide, nitrite, and nitric oxide were expected as products under nitrate reduction at −0.2 V (vs. SCE). In this work, nitrite was formed after 1 h in the present of nitrate; however, nitrogen dioxide and nitric oxide were not observed. This might be caused by the fast reduction from nitrate to nitrogen dioxide and nitric oxide to nitrite [46]. Note that ammonium was detected (Fig. 8b) because its redox potential is overlapped with the edge of nitrogen gas-to-ammonia peak. At the potential equal to −0.23 V (vs. SCE) (Fig. 8c), both nitrite and ammonium were formed in the first two hours. Afterward, it was noted that the ammonium concentration continued to increase whereas the nitrite concentration decreased, which suggested clearly that there was reaction between nitrite and ammonium to yield molecular nitrogen, that is, $NO_2^- + NH_4^+ = N_2(g) + 2H_2O$. Additionally, the nitrogen concentration increased from the forth hour while the concentration of ammonium reached a steady-state. The result might be due to the nitrite-to-nitric oxide and nitric oxide-to-nitrogen reaction and the suppression of the ammonium formation by nitric oxide and nitrogen due to the potential preference. According to Ramsier et al. [47] and de Vooys et al. [21], it is thermodynamically possible to reduce nitrite to nitrogen rather than ammonium.

As the applied potential was changed to −0.3 V (vs. SCE), the trend of nitrate reduction product (nitrite, and ammonia) was similar to that at −0.23 V (vs. SCE). The concentration of the ammonia reached a plateau while nitrite concentration continued to decrease. Notably, the yield of nitrite at −0.3 V (vs. SCE) was two times lower than that at −0.23 V (vs. SCE), because of hydrogen generation, which was favored at high potential that hindered the adsorption of nitrate on the electrode surface [16,34,48]. Additionally, the increase in hydrogen population on the electrode surface was reported to promote the production of ammonia [49], which was also consistent with the experimental data shown in Fig. 8d. Furthermore, the loss of N concentration was due to the nitrous oxide-to-nitrogen reduction per the reduction potential. Comparing the results shown in Fig. 8b and Fig. 8d, nitrate was almost completely reduced at the reduction potential of 0.3 V (vs. SCE). While only 40% of nitrite was produced at −0.2 V (vs. SCE). It was clear that the reduction rate of nitrate-to-nitrite strongly was dependent on the applied potential. Furthermore, results in (Fig. 8a–d) also demonstrates that the applied potential in nitrate reduction is one of the key factors governing the reaction efficiency.

According to the experimental results (Fig. 8a–d) of the present study and reported elsewhere in the literature [45,50,51], the following mechanism of nitrate reduction in aqueous solutions over Pd–Cu/SS electrode was proposed:

$$NO_3^- + S_1 = S_1NO_3^- \quad (14)$$

$$S_2 + H_2O = S_2H_2O \quad (15)$$

$$S_2H_2O + e = S_2H + HO \quad (16)$$

$$S_1NO_3^- + 2S_2H \rightarrow S_1NO_2^- + S_2H_2O + S_2 \quad (17)$$

$$S_1NO_3^- + 2e \rightarrow S_1NO_2^- + O \quad (18)$$

$$S_1NO_2^- + NO_2^- + S_1 \quad (19)$$

$$NO_2^- + S_2 = S_2NO_2^- \quad (20)$$

$$S_2NO_2^- + S_2H \rightarrow S_2NO + OH^- + S_2 \quad (21)$$

$$S_2NO_2^- + e \rightarrow S_2NO + O^- \quad (22)$$

$$2S_2NO \rightarrow S_2N_2O + S_2 + O \quad (23)$$

$$2S_2NO + 2e \rightarrow S_2N_2O + O + S_2 \quad (24)$$

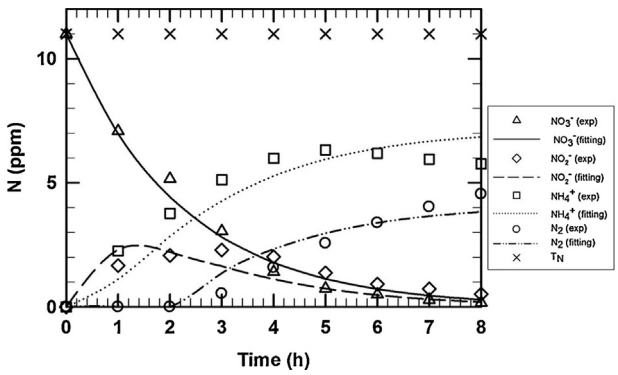

Fig. 9. The variation of various nitrogen species as a function of reaction time shown in Fig. 8d as fitted by the proposed reaction mechanism over the Pd–Cu/SS electrode.

$$S_2N_2O + S_2H \rightarrow S_2N_2 + S_2OH \quad (25)$$

$$S_2N_2O + e \rightarrow S_2N_2 + O \quad (26)$$

$$S_2N_2 + e \rightarrow S_2 + N_2 \quad (27)$$

$$S_2NO + S_2H \rightarrow S_2HN + S_2 + O \quad (28)$$

$$S_2HN + S_2H \rightarrow S_2H_2N + S_2 \quad (29)$$

$$S_2H_2N + S_2H \rightarrow S_2H_3N + S_2 \quad (30)$$

$$S_2H_3N \rightarrow NH_3 + S_2 \quad (31)$$

$$NH_3 + H_2O = NH_4^+ + OH^- \quad (32)$$

$$S_2OH + S_2H \rightarrow H_2O + 2S_2 \quad (33)$$

$$S_2H + S_2H = 2S_2 + H_2 \quad (34)$$

$$O + S_1 = S_1O \quad (35)$$

$$S_1O + S_1O \rightarrow O_2 + 2S_1 \quad (36)$$

where S_1 denotes a vacant surface Cu site and S_2 represents a vacant surface Pd site on the Pd–Cu/SS electrode. The key features of the above reaction scheme are: (1) adsorption of NO_3^- onto an empty copper site; (2) the surface reduction of nitrate to nitrite; (3) the adsorption of H_2O on the empty palladium site which is then reduced to yield hydrogen atom; (4), the adsorption of NO_2^- on to the empty palladium site, which can occur directly from site jumping from the copper to the palladium site; (5) a series of surface reaction involved the surface hydrogen atom (on the palladium site) with various surface oxy-nitrogen species eventually lead to the production of nitrogen molecules; (6) further reaction by the surface hydrogen species eventually yield ammonia.

Based on the above reaction steps, the temporal concentration of major reaction products and nitrate can be derived (Supporting information). The temporal concentration of nitrate, nitrite, nitrogen gas, and ammonium were as the following.

$$C_{NO_3^-} = C^0_{NO_3^-} e^{-k' t} \quad (37)$$

$$C_{NO_2^-} = \frac{k' C^0_{NO_3^-}}{k'' + k''' - k'} [e^{-k' t} - e^{-(k''+k''')t}] \quad (38)$$

$$C_{N_2} = \frac{k'' C^0_{NO_3^-}}{k'' + k''' - k'} (e^{-2k'} - e^{-k' t}) + \frac{k' k'' C^0_{NO_3^-}}{(k'' + k''' - k')(k'' + k''')} [e^{-(k''+k''')t} - e^{-(k''+k''')2}] \quad (39)$$

$$C_{NH_4^+} = \frac{k''' k'''' C^0_{NO_3^-}}{k'' + k''' - k'} (1 - e^{-k' t}) + \frac{k' k''' k'''' C^0_{NO_3^-}}{(k'' + k''' - k')(k'' + k''')} [e^{-(k''+k''')t} - 1] \quad (40)$$

Eqs. (37)–(40) were fitted to the concentration data (nitrate, nitrite, nitrogen gas, and ammonium) in Fig. 8d and the fitting result was shown in Fig. 9. The fitting parameters, k', k'', k''', and k'''', were obtained using the minimal residuals method. The fitted kinetic constants were: $k' = 0.45(h^{-1})$, $k'' = 0.70(h^{-1})$, $k''' = 0.43(h^{-1})$, and $k'''' = 1.72$. The agreement between the fitted and the experimental data shown in Fig. 9 confirmed the validity of the proposed mechanism of nitrate reduction.

4. Conclusions

The electrochemical reduction of nitrate could be studied using a combination of cyclic voltammetry and direct chemical analysis. The reduction potential of different nitrate reduction couples were analyzed with cyclic voltammetry. The nitrate reduction was significantly influenced by the electrode material and the applied potential. The voltammetric results demonstrated that the bimetallic Pd–Cu/SS electrode remarkably enhanced the reactivity toward nitrite reduction. Moreover, the corresponding SEM micrographs revealed that the Cu/SS and Pd–Cu/SS electrode exhibited a polyhedral crystal and dendrite structure, respectively. Such difference in electrode crystal structure might also contribute to the different reaction mechanisms between Cu/SS and Pd–Cu/SS electrode. In addition, results showed that it is possible to manipulate the nitrate reduction product by controlling the applied potential and electrode material. Furthermore, results also provided a significant step forward in designing and developing a novel and efficient method for nitrate removal.

Acknowledgement

We wish to express our gratitude to the Department of Civil and Environmental Engineering, University of Delaware, for the support of a graduate research fellowship (to JF Su).

Appendix A. Supplementary data

Supplementary data associated with this article can be found, in the online version, at http://dx.doi.org/10.1016/j.apcatb.2015.06.028

References

[1] S.R. Carpenter, N.F. Caraco, D.L. Correll, R.W. Howarth, A.N. Sharpley, V.H. Smith, Nonpoint pollution of surface waters with phosphorus and nitrogen, Ecol. Appl. 8 (1998) 559–568.
[2] W. Huang, M. Li, B. Zhang, C. Feng, X. Lei, B. Xu, Influence of operating conditions on electrochemical reduction of nitrate in groundwater, Water Environ. Res. 85 (2013) 224–231.
[3] Y. Fernández-Nava, E. Marañón, J. Soons, L. Castrillón, Denitrification of wastewater containing high nitrate and calcium concentrations, Bioresour. Technol. 99 (2008) 7976–7981.
[4] W.H. Organization, Rolling revision of the WHO Guidelines for drinking-waters quality, Nitrates and Nitrites in Drinking-Waters, (2004).
[5] A. Corma, A.E. Palomares, F. Rey, J.G. Prato, Catalytic reduction of nitrates in natural water: is this a realistic objective, J. Catal. 227 (2004) 561–562.
[6] V. Matějů, S. Čižinská, J. Krejčí, T. Janoch, Biological water denitrification—a review, Enzyme Microb. Technol. 14 (1992) 170–183.
[7] I. Mikami, Y. Sakamoto, Y. Yoshinaga, T. Okuhara, Kinetic and adsorption studies on the hydrogenation of nitrate and nitrite in water using Pd–Cu on active carbon support, Appl. Catal. B Environ. 44 (2003) 79–86.

[8] Y. Yoshinaga, T. Akita, I. Mikami, T. Okuhara, Hydrogenation of nitrate in water to nitrogen over Pd–Cu supported on active carbon, J. Catal. 207 (2002) 37–45.
[9] F. Deganello, L.F. Liotta, A. Macaluso, A.M. Venezia, G. Deganello, Catalytic reduction of nitrates and nitrites in water solution on pumice-supported Pd–Cu catalysts, Appl. Catal. B Environ. 24 (2000) 265–273.
[10] W. Gao, N. Guan, J. Chen, X. Guan, R. Jin, H. Zeng, Z. Liu, F. Zhang, Titania supported Pd–Cu bimetallic catalyst for the reduction of nitrate in drinking water, Appl. Catal. B: Environ. 46 (2003) 341–351.
[11] A. Kapoor, T. Viraraghavan, Nitrate removal from drinking water—review, J. Environ. Eng. 123 (1997) 371–380.
[12] K.-D. Vorlop, T. Tacke, Erste Schritte auf dem Weg zur edelmetallkatalysierten Nitrat- und Nitrit-Entfernung aus Trinkwasser, Chem. Ing. Tech. 61 (1989) 836–837.
[13] J.G.I. Krishnan Rajeshwar, Environ. Electrochem. Fundam. Appl. Pollut. Sens. Abatement (1997) 776.
[14] O. Ghodbane, M. Sarrazin, L. Roué, D. Bélanger, Electrochemical reduction of nitrate on pyrolytic graphite-supported Cu and Pd–Cu electrocatalysts, J. Electrochem. Soc. 155 (2008) F117–F123.
[15] M. Li, C. Feng, Z. Zhang, Z. Shen, N. Sugiura, Electrochemical reduction of nitrate using various anodes and a Cu/Zn cathode, Electrochem. Commun. 11 (2009) 1853–1856.
[16] M.S. El-Deab, Electrochemical reduction of nitrate to ammonia at modified gold electrodes, Electrochim. Acta 49 (2004) 1639–1645.
[17] J. Qu, X. Zhao, Design of BDD-TiO_2 hybrid electrode with P–N function for photoelectrocatalytic degradation of organic contaminants, Environ. Sci. Technol. 42 (2008) 4934–4939.
[18] G. Zhao, Y. Zhang, Y. lei, B. Lv, J. Gao, Y. Zhang, D. Li, Fabrication and electrochemical treatment application of a novel lead dioxide anode with superhydrophobic surfaces, high oxygen evolution potential, and oxidation capability, Environ. Sci. Technol. 44 (2010) 1754–1759.
[19] O.W.J.S. Rutten, A.V. Sandwijk, G.V. Weert, The electrochemical reduction of nitrate in acidic nitrate solutions, J. Appl. Electrochem. 29 (1999) 87–92.
[20] M. Li, C. Feng, Z. Zhang, X. Lei, R. Chen, Y. Yang, N. Sugiura, Simultaneous reduction of nitrate and oxidation of by-products using electrochemical method, J. Hazard. Mater. 171 (2009) 724–730.
[21] A.C.A. de Vooys, R.A. van Santen, J.A.R. van Veen, Electrocatalytic reduction of NO_3- on palladium/copper electrodes, J. Mol. Catal. A Chem. 154 (2000) 203–215.
[22] J.O.M. Bockris, J. Kim, Electrochemical reductions of Hg(II), ruthenium-nitrosyl complex, chromate, and nitrate in a strong alkaline solution, J. Electrochem. Soc. 143 (1996) 3801–3808.
[23] H.L. Li, J.Q. Chambers, D.T. Hobbs, Electroreduction of nitrate ions in concentrated sodium hydroxide solutions at lead, zinc, nickel and phthalocyanine-modified electrodes, J. Appl. Electrochem. 18 (1988) 454–458.
[24] H. l. Li, D.H. Robertson, J.Q. Chambers, D.T. Hobbs, Electrochemical reduction of nitrate and nitrite in concentrated sodium hydroxide at platinum and nickel electrodes, J. Electrochem. Soc. 135 (1988) 1154–1158.
[25] J.O.M. Bockris, J. Kim, Electrochemical treatment of low-level nuclear wastes, J. Appl. Electrochem. 27 (1997) 623–634.
[26] K. Bouzek, M. Paidar, A. Sadílková, H. Bergmann, Electrochemical reduction of nitrate in weakly alkaline solutions, J. Appl. Electrochem. 31 (2001) 1185–1193.
[27] N. Chebotareva, T. Nyokong, Metallophthalocyanine catalysed electroreduction of nitrate and nitrite ions in alkaline media, J. Appl. Electrochem. 27 (1997) 975–981.
[28] M. Paidar, I. Roušar, K. Bouzek, Electrochemical removal of nitrate ions in waste solutions after regeneration of ion exchange columns, J. Appl. Electrochem. 29 (1999) 611–617.
[29] S. Ureta-Zañartu, C. Yáñez, Electroreduction of nitrate ion on Pt, Ir and on 70:30 Pt:Ir alloy, Electrochim. Acta 42 (1997) 1725–1731.
[30] G. Horányi, E.M. Rizmayer, Indirect radiotracer study of the adsorption of NO_3 ions at a platinized platinum electrode in acidic medium, J. Electroanal. Chem. Interfacial Electrochem. 188 (1985) 273–279.
[31] G.E. Dima, A.C.A. de Vooys, M.T.M. Koper, Electrocatalytic reduction of nitrate at low concentration on coinage and transition-metal electrodes in acid solutions, J. Electroanal. Chem. 554–555 (2003) 15–23.
[32] J.F.E. Gootzen, L. Lefferts, J.A.R. van Veen, Electrocatalytic nitrate reduction on palladium based catalysts activated with germanium, Appl. Cata. A Gen. 188 (1999) 127–136.
[33] D. Reyter, D. Bélanger, L. Roué, Study of the electroreduction of nitrate on copper in alkaline solution, Electrochim. Acta 53 (2008) 5977–5984.
[34] L. Szpyrkowicz, S. Daniele, M. Radaelli, S. Specchia, Removal of NO_3- from water by electrochemical reduction in different reactor configurations, Appl. Catal. B Environ. 66 (2006) 40–50.
[35] D.M. Wang, C.P. Huang, J.G. Chen, H.Y. Lin, S.I. Shah, Reduction of perchlorate in dilute aqueous solutions over monometallic nano-catalysts: exemplified by tin, Sep. Purif. Technol. 58 (2007) 129–137.
[36] L.-J. Zhang, H.-C. Tao, X.-Y. Wei, T. Lei, J.-B. Li, A.-J. Wang, W.-M. Wu, Bioelectrochemical recovery of ammonia–copper(II) complexes from wastewater using a dual chamber microbial fuel cell, Chemosphere 89 (2012) 1177–1182.
[37] J.F. Löffler, J. Schroers, W.L. Johnson, Time–temperature–transformation diagram and microstructures of bulk glass forming $Pd_{40}Cu_{30}Ni_{10}P_{20}$, Appl. Phys. Lett. 77 (2000) 681–683.
[38] J. Liu, X. Li, Q. Zhao, D. Zhang, P. Ndokoye, The selective catalytic reduction of NO with propene over Cu-supported Ti–Ce mixed oxide catalysts: Promotional effect of ceria, J. Mol. Catal. A Chem. 378 (2013) 115–123.
[39] S. Bae, J. Jung, W. Lee, The effect of pH and zwitterionic buffers on catalytic nitrate reduction by TiO_2-supported bimetallic catalyst, Chem. Eng. J. 232 (2013) 327–337.
[40] L.R.F. Allen, J. Bard, Electrochemical Methods: Fundamentals and Applications, 2nd Edition, (2000) 95.
[41] D. De, J.D. Englehardt, E.E. Kalu, Cyclic voltammetric studies of nitrate and nitrite ion reduction at the surface of iridium-modified carbon fiber electrode, J. Electrochem. Soc. 147 (2000) 4224–4228.
[42] A.M.O.B. Christopher, M.A. Brett, Electrochemistry, Principles, Methods and Applications, (1993).
[43] D. Reyter, D. Beílanger, L. Roueí, Elaboration of Cu–Pd films by coelectrodeposition: application to nitrate electroreduction, J. Phys. Chem. C 113 (2008) 290–297.
[44] A. Ruban, B. Hammer, P. Stoltze, H.L. Skriver, J.K. Nørskov, Surface electronic structure and reactivity of transition and noble metals, J. Mol. Catal. A Chem. 115 (1997) 421–429.
[45] U. Prüsse, K.-D. Vorlop, Supported bimetallic palladium catalysts for water-phase nitrate reduction, J. Mol. Catal. A Chem. 173 (2001) 313–328.
[46] P. Neta, R.E. Huie, A.B. Ross, Rate constants for reactions of inorganic radicals in aqueous solution, J. Phys. Chem. Ref. Data 17 (1988) 1027–1284.
[47] R.D. Ramsier, Q. Gao, H.N. Waltenburg, K.W. Lee, O.W. Nooij, L. Lefferts, J.T. Yates Jr, NO adsorption and thermal behavior on Pd surfaces. A detailed comparative study, Surf. Sci. 320 (1994) 209–237.
[48] O. Brylev, M. Sarrazin, L. Roué, D. Bélanger, Nitrate and nitrite electrocatalytic reduction on Rh-modified pyrolytic graphite electrodes, Electrochim. Acta 52 (2007) 6237–6247.
[49] O.S.G.P. Soares, X. Fan, J.J.M. Órfão, A.A. Lapkin, M.F.R. Pereira, Kinetic modeling of nitrate reduction catalyzed by Pd–Cu supported on carbon nanotubes, Ind. Eng. Chem. Res. 51 (2012) 4854–4860.
[50] A. Pintar, J. Batista, J. Levec, T. Kajiuchi, Kinetics of the catalytic liquid-phase hydrogenation of aqueous nitrate solutions, Appl. Catal. B: Environ. 11 (1996) 81–98.
[51] J. Warna, I. Turunen, T. Salmi, T. Maunula, Kinetics of nitrate reduction in monolith reactor, Chem. Eng. Sci. 49 (1994) 5763–5773.